Improving the conditioning of the Method of Fundamental Solutions for the Helmholtz equation on domains in polar or elliptic coordinates

Pedro R. S. Antunes[a,b], Hernani Calunga[a,c,*], Pedro Serranho[c,d,e]

[a] *GFM - Group of Mathemathical Physics, Instituto Superior Técnico, University of Lisbon, Av. Rovisco Pais 1, 1049-001 Lisbon, Portugal*
[b] *Department of Mathematics, Instituto Superior Técnico, University of Lisbon, Av. Rovisco Pais 1, 1049-001 Lisbon, Portugal*
[c] *DCeT - Department of Sciences and Technology, Universidade Aberta, Rua da Escola Politécnica 141-147, 1269-001 Lisbon, Portugal*
[d] *CIBIT - Coimbra Institute for Biomedical Imaging and Translational Research, University of Coimbra, Polo III, Azinhaga de Santa Comba, Celas, 3000-548 Coimbra, Portugal*
[e] *CEMAT - Center for Computational and Stochastic Mathematics, University of Lisbon, Av. Rovisco Pais 1, 1049-001 Lisbon, Portugal*

Abstract

A new approach to overcome the ill-conditioning of the Method of Fundamental Solutions (MFS) combining Singular Value Decomposition (SVD) and an adequate change of basis was introduced in [1] as MFS-SVD. The original formulation considered polar coordinates and harmonic polynomials as basis functions and is restricted to the Laplace equation in 2D. In this work, we start by adapting the approach to the Helmholtz equation in 2D and later extending it to elliptic coordinates. As in the Laplace case, the approach in polar coordinates has very good numerical results both in terms of conditioning and accuracy for domains close to a disk but does not perform so well for other domains, such as an eccentric ellipse. We therefore consider the MFS-SVD approach in elliptic coordinates with Mathieu functions as basis functions for the latter. We illustrate the feasibility of the approach by numerical examples in both cases.

Keywords:
Method of fundamental solutions, Helmholtz equation, MFS-SVD, addition

*Corresponding author

Email addresses: `prsantunes@tecnico.ulisboa.pt` (Pedro R. S. Antunes), `2001757@estudante.uab.pt` (Hernani Calunga), `Pedro.Serranho@uab.pt` (Pedro Serranho)

theorem, ill-conditioning, Mathieu functions

1. Introduction

The Method of Fundamental Solutions (MFS) is a meshless numerical method introduced more than half a century ago by Kupradze and Aleksidze [2], quite often used to solve boundary value problems for partial differential equations whose fundamental solution is known. This collocation method looks for a linear combination of shifts of the fundamental solution of the given differential operator with source points on an admissible source set.

The MFS is known to be highly accurate, specially on analytic domains [3] and has a simple computational implementation; due to this, applications in several areas such as fluid mechanics [4, 5], elasticity [6, 7], acoustics [3, 8], electromagnetism [9, 10], stationary heat conduction [11] and option pricing [12] have been employed. However, the previously mentioned high accuracy is sometimes compromised as the linear system is often highly ill-conditioned. Therefore, the use of regularization techniques is normally required to obtain a stable MFS approximation to the solution. There exists a variety of techniques for regularization, such as Tikhonov regularization [13], Singular Value Decomposition [14, 15], QR decomposition [16, 17], but still the research on approaches to overcome the ill-conditioning of the MFS is very active, both in general or more specific cases [1, 16–18].

An alternative approach to overcome the ill-conditioning is changing the basis functions to a more adequate set. In [1] a well-conditioned algorithm named the MFS-SVD was introduced, which finds a new set of basis functions based on harmonic polynomials, spanning the same approximation space as the original one and reducing the ill-conditioning of the MFS when applied to boundary value problems for the Laplace equation.

In this work, we look for generalizations of the MFS-SVD approach both for the Helmholtz equation and other geometries described in different systems of coordinates. In particular, we are interested in domains in polar and elliptic coordinates. To this end we explore Mathieu functions as the basis functions for problems involving elliptic coordinates, as we noticed that the expansion in terms of Bessel functions used for polar coordinates has limited improvement for elliptic domains.

The paper is organized as follows. In section 2 we present the boundary value problem to be solved and describe the standard approach to find its numerical solution by MFS. In section 3 we detail the MFS-SVD approach in polar coordinates and in section 4 the MFS-SVD approach in elliptic coordinates. In section 5 we present some numerical results to illustrate the feasibility of the method, both in terms of reducing the ill-conditioning and therefore attaining better accuracy . Finally, in section 6 we summarize our findings and draw some conclusions. At the end we added an appendix summarizing some aspects of Mathieu functions, needed in the paper.

2. The Method of Fundamental Solutions

Let D be a bounded and smooth domain in $\mathbb{R}^2$ whose boundary is denoted by ∂D. We consider the following Dirichlet boundary value problem for the Helmholtz equation

$$\begin{cases} \Delta u + k^2 u = 0 \quad \text{in} \quad D, \\ u = g \quad \text{on} \quad \partial D, \end{cases} \tag{1}$$

for the unknown field u, with a given function $g \in H^{1/2}(\partial D)$ and wavenumber $k > 0$.

In order to solve numerically this problem by the MFS, we recall that the fundamental solution for the Helmholtz operator in $\mathbb{R}^2$ is given by

$$\Phi(x) = \frac{i}{4} H_0^{(1)}(k|x|), \quad x \neq 0, \tag{2}$$

where $H_0^{(1)}$ is the Hankel function of the first kind of order zero. The classical MFS [19–23] states that an approximation u for the solution of the problem (1) can be obtained through a linear combination of a set of basis functions $\Phi(\cdot - y_j)$, where $y_j \in C, j = 1, 2, ..., N$, represent points over the closed curve C, which is the boundary of a bounded open domain containing $\bar{D}$. As in [16], let us refer to the classical approach as Direct MFS. Therefore an approximation to the solution of our problem can be obtained by

$$u_N^D(x) = \sum_{n=1}^{N} \mathrm{a}_n^D \Phi(x - y_n), \quad x \in \bar{D}, \quad y_n \in C, \tag{3}$$

for some coefficients $\mathrm{a}_n^D \in \mathbb{C}$. Due to properties of the fundamental solution, the representation (3) for the field u_N^D satisfies the Helmholtz equation in D and the accurate approximation of the boundary condition by the same representation can be justified by density results, since

$$span\left\{ \Phi(\cdot - y)|_D : y \in C \right\}$$

is dense in $\{\nu \in H^1(D) : (\Delta + k^2)\nu = 0\}$, with H^1 topology [8].

Assuming that we have N points $y_j \in C$, then the coefficients can be determined by collocation, by forcing the boundary condition to be satisfied at the points $x_i \in \partial D, i = 1, 2, ..., M$. By doing so, the problem is then reduced to solving a linear system for the coefficients a_n^D which for $M > N$ is an overdetermined system written as

$$\mathbf{A}^D \mathbf{a}^D = \mathbf{G}, \tag{4}$$

with entries given by

$$A_{i,j} = \Phi(x_i - y_j), \quad a_j = \mathrm{a}_j^D, \quad G_i = g(x_i), \quad i = 1, 2, ..., M, \quad j = 1, 2, ..., N.$$

The MFS approach described above is usually highly accurate for analytic domains, but the linear system (4) solved in the least squares sense is often severely ill-conditioned; therefore one needs to find strategies to deal with the ill-conditioning.

In the following section we follow similar steps to those in the MFS-SVD approach for the Laplace equation [1] extending it to the Helmholtz case for polar coordinates and later to elliptic coordinates.

3. The MFS-SVD formulation in polar coordinates

In this section we generalize the approach introduced in [1] for the Laplace equation to the Helmholtz equation in polar coordinates, which we denote by MFS-SVD$_P$. We start by decomposing the fundamental solution into a sum of products of terms depending separately on the evaluation and source points, through Graf's addition theorem [16, 24]

$$H_0^{(1)}(k|x - y|) = H_0^{(1)}(k|y|)J_0(k|x|) + 2\sum_{n=1}^{\infty} H_n^{(1)}(k|y|)J_n(k|x|)\cos(n\beta), \quad |y| > |x|, \tag{5}$$

with β denoting the angle between x and y. Expression (5) can be written in polar coordinates, assuming $x = (r_P, \theta)$, $y_j = (R_{P,j}, \alpha_j)$, $\Psi_j(r_P, \theta) := \Phi(x - y_j)$, $j = 1, 2, ..., N$, as

$$\begin{aligned} \Psi_j(r_P, \theta) = {} & H_0^{(1)}(kR_{P,j})J_0(kr_P) + \\ & 2\sum_{n=1}^{\infty} H_n^{(1)}(kR_{P,j})J_n(kr_P)\Big(\cos(n\theta)\cos(n\alpha_j) + \sin(n\theta)\sin(n\alpha_j)\Big) \quad R_{P,j} > r_P. \end{aligned} \tag{6}$$

Therefore, dropping $i/4$ from the fundamental solution to be incorporated in the coefficients of the MFS one has the operator decomposition for the array of basis functions given by

$$\Theta_\infty(r_P, \theta, \mathbf{R}_P, \boldsymbol{\alpha}) = \begin{bmatrix} \Psi_1(r_P, \theta, R_{P,1}, \alpha_1) \\ \Psi_2(r_P, \theta, R_{P,2}, \alpha_2) \\ \vdots \\ \Psi_N(r_P, \theta, R_{P,N}, \alpha_N) \end{bmatrix}$$

$$= \begin{bmatrix} B^1_{p,0} & B^1_{p,1} & B^1_{p,2} & B^1_{p,3}\cdots \\ B^2_{p,0} & B^2_{p,1} & B^2_{p,2} & B^2_{p,3}\cdots \\ \vdots & \vdots & \vdots & \vdots \\ B^N_{p,0} & B^N_{p,1} & B^N_{p,2} & B^N_{p,3}\cdots \end{bmatrix} \begin{bmatrix} J_0(kr_P)/J^*_0 \\ J_1(kr_P)/J^*_1 \cos(\theta) \\ J_1(kr_P)/J^*_1 \sin(\theta) \\ J_2(kr_P)/J^*_2 \cos(2\theta) \\ J_2(kr_P)/J^*_2 \sin(2\theta) \\ J_3(kr_P)/J^*_3 \cos(3\theta) \\ J_3(kr_P)/J^*_3 \sin(3\theta) \\ \vdots \end{bmatrix}$$

$$= \mathbf{B}_{P,\infty}(\mathbf{R}_P, \boldsymbol{\alpha})\mathbf{F}_{P,\infty}(r_P, \theta), \tag{7}$$

where

$$B^j_{p,0} = \left[H^{(1)}_0(kR_{P,j})J^*_0\right], B^j_{p,n} = \left[2H^{(1)}_n(kR_{P,j})J^*_n \cos(n\alpha_j) \quad 2H^{(1)}_n(kR_{P,j})J^*_n \sin(n\alpha_j)\right],$$

$$r_D := \min_{x\in\partial D}||x||,\ R_D := \max_{x\in\partial D}||x||,\ J^*_n = \max_{r\in[r_D,R_D]}|J_n(kr)|, \tag{8}$$

for $n = 1, 2, ...$ and $j = 1, 2, ..., N$.

When the expansion (5) is truncated for some $T_P \in \mathbb{N}$, then (7) can be written as

$$\Theta(r_P, \theta, \mathbf{R}_P, \boldsymbol{\alpha}) = \mathbf{B}_P(\mathbf{R}_P, \boldsymbol{\alpha})\mathbf{F}_P(r_P, \theta) \tag{9}$$

with T_P such that $2T_P + 1 \geq N$ so that $\mathbf{B}_P(\mathbf{R}_P, \boldsymbol{\alpha})$ has at least as many columns as rows.

As in [1], we proceed by computing the singular value decomposition of $\mathbf{B}_P$,

$$\mathbf{B}_P = \mathbf{USV}^*, \tag{10}$$

with $\mathbf{U}$ and $\mathbf{V}$ being unitary and $\mathbf{S}$ diagonal with non negative entries. Multiplying from the left by $\mathbf{U}^*$ we get

$$\mathbf{U}^*\mathbf{B}_P = \mathbf{U}^*\mathbf{U}\mathbf{S}\mathbf{V}^* = \mathbf{I}\mathbf{S}\mathbf{V}^* = \mathbf{S}\mathbf{V}^*. \tag{11}$$

Since we have chosen T_P such that $2T_P + 1 \geq N$ then we can write

$$\mathbf{S} = [\mathbf{S}_1|\mathbf{0}],$$

where $\mathbf{S}_1$ is a square matrix and $\mathbf{0}$ denotes a block matrix with all entries equal to zero. It follows that,

$$\mathbf{S}\mathbf{V}^* = [\mathbf{S}_1|\mathbf{0}]\left[\frac{\mathbf{V}_1^*}{\mathbf{V}_2^*}\right] = \mathbf{S}_1\mathbf{V}_1^*,$$

where $\mathbf{V}_1^*$ is the matrix composed of the first N rows of $\mathbf{V}^*$. Now, multiplying from the left by the matrix $\mathbf{S}_1^{-1}$ from (11) we obtain

$$\mathbf{S}_1^{-1}\mathbf{U}^*\mathbf{B}_P = \mathbf{S}_1^{-1}\mathbf{S}\mathbf{V}^* = \mathbf{S}_1^{-1}\mathbf{S}_1\mathbf{V}_1^* = \mathbf{V}_1^*.$$

This shows that we obtain a new set of basis functions $\varphi(r_P, \theta)$ by multiplying by $\mathbf{S}_1^{-1}\mathbf{U}^*$ from the left, therefore obtaining

$$\varphi(r_P, \theta) = \left(\mathbf{S}_1^{-1}\mathbf{U}^*\right)\Theta(r_P, \theta, \mathbf{R}_P, \boldsymbol{\alpha}) = \mathbf{V}_1^*\mathbf{F}(r_P, \theta). \tag{12}$$

To take advantage of the better numerical conditioning one should now use the new basis functions computed using the last matrix product in (12).

The MFS-SVD$_P$ approach is the approximation obtained by a linear combination of the new basis function $\varphi(r_P, \theta)$,

$$u_N^{SVD}(r_P, \theta) = \sum_{n=1}^{N} \mathrm{a}_n^{SVD}\varphi_n(r_P, \theta). \tag{13}$$

The coefficients can be determined by solving

$$\mathbf{A}^P\mathbf{a}^{SVD} = \mathbf{G}, \tag{14}$$

where,
$\mathbf{A}^P = \varphi(x_i)^T = [\varphi(x_1), \varphi(x_2), ..., \varphi(x_N)]^T$ and $\mathbf{a}^{SVD} = [\mathrm{a}_1^{SVD}, \mathrm{a}_2^{SVD}, ..., \mathrm{a}_N^{SVD}]^T$.

Remark 1. Note that as $N \leq 2T_P + 1$, an increasing number of source points N leads to an increasing truncation number T_P. This may raise underflow problems, due to the asymptotic limit tending to zero of the Bessel function J_n with increasing n, when computing the ratios J_n/J_n^* from a certain $n \geq N^*$. To avoid this, for N greater than a fixed N^*, the ratio J_n/J_n^* is computed using the asymptotic behavior [25] given by

$$J_n(z) \sim \frac{1}{\sqrt{2\pi n}} \left(\frac{ez}{2n} \right)^n, \quad n \longrightarrow \infty. \tag{15}$$

4. The MFS-SVD formulation in elliptic coordinates

As we will see in section 5, the MFS-SVD$_P$ approach takes care of the ill-conditioning for disks, but it has mild effect for domains with less symmetry than the disk, in particular for domains that are elongated in one direction.

Let us consider the problem (1) with D being a domain defined by an ellipse. In this situation, it is clear that the geometry of the domain is better described using elliptic coordinates, and Mathieu functions will be a natural choice for the basis functions instead of the Bessel functions used for the disk.

In this section, we illustrate how to formulate the MFS-SVD approach when considering domains described in elliptic coordinates. We will denote this case as MFS-SVD$_E$.

The elliptic coordinate system can be defined as in [26] by

$$x_1 = \sigma \cosh \eta \cos \nu, \quad x_2 = \sigma \sinh \eta \sin \nu, \tag{16}$$

where, $\sigma > 0$, $0 \leq \eta < \infty$ and $0 \leq \nu \leq 2\pi$. If $\eta = \eta_0$ from (16) we obtain the ellipse

$$\frac{x_1^2}{\sigma^2 \cosh^2 \eta_0} + \frac{x_2^2}{\sigma^2 \sinh^2 \eta_0} = 1, \tag{17}$$

with semi axes $a = \sigma \cosh \eta_0$ and $b = \sigma \sinh \eta_0$. When the two semi axes of the ellipse are known then

$$\eta_0 = \tanh^{-1} \frac{b}{a}, \quad \sigma = \sqrt{a^2 - b^2}. \tag{18}$$

To transform the cartesian coordinates (x_1, x_2) to elliptic coordinates (η, ν) the following explicit transformations are used

$$\eta = \sinh^{-1} F(x_1, x_2, \sigma), \quad \nu = \cos^{-1} \left(\frac{x_1}{\sigma \cosh \eta} \right), \tag{19}$$

with

$$F(x_1,x_2,\sigma)=\frac{1}{\sqrt{2}\sigma}\sqrt{(x_1^2+x_2^2-\sigma^2)+\sqrt{(x_1^2+x_2^2-\sigma^2)^2+4\sigma^2x_2^2}}.$$

When $x_2 \geq 0$ from (19) we get $0 \leq \nu \leq \pi$ while if $x_2 < 0$ we get $\pi < \nu < 2\pi$, [27].

We aim to solve (1) by transforming the problem from cartesian to elliptic coordinates. Let both $x \in \partial D$ and $y \in C$, be represented in the same elliptic coordinate system. We consider the elliptic coordinates for x and y given by $x = (r_E, \vartheta)$ and $y = (R_E, \omega)$.

The Hankel function (5) is expressed in elliptic coordinates by a series expansion containing Mathieu functions [28, 29] as

$$\begin{aligned}H_0^{(1)}(k|x-y|) = 4\sum_{n=0}^{\infty}\Bigg(&\frac{1}{Ne_n}\mathrm{Re}_n^{(1)}(q,r_E)\mathrm{Re}_n^{(3)}(q,R_E)\mathrm{Se}_n(q,\vartheta)\mathrm{Se}_n(q,\omega)+\\ &\frac{1}{No_n}\mathrm{Ro}_n^{(1)}(q,r_E)\mathrm{Ro}_n^{(3)}(q,R_E)\mathrm{So}_n(q,\vartheta)\mathrm{So}_n(q,\omega)\Bigg),\ R_E > r_E,\end{aligned} \qquad (20)$$

where $q = k^2\sigma^2/4$, Se_n and So_n are the even and odd angular Mathieu functions, $\mathrm{Re}_n^{(1)}$, $\mathrm{Re}_n^{(3)}$ the even radial Mathieu functions of first and third kind, $\mathrm{Ro}_n^{(1)}$and $\mathrm{Ro}_n^{(3)}$ are the odd radial Mathieu functions of first and third kind, and $Ne_n$and No_n are the even and odd normalization coefficients, respectively, whose definitions can be found in the appendix (see section 7). The series expansion (20) is to be considered for both cases of the even Mathieu functions and the odd Mathieu functions, that is, we will have four terms for each term in the sum. Note that, among the several notations used to denote Mathieu functions, in this work we use the Stratton convention.

Now, by following the same rationale as in section 3, we can write

$$\begin{aligned}\Xi_\infty(r_E,\vartheta,\mathbf{R}_E,\boldsymbol{\omega}) = \begin{bmatrix}\Lambda_1(r_E,\vartheta,R_{E,1},\omega_1)\\ \Lambda_2(r_E,\vartheta,R_{E,2},\omega_2)\\ \vdots\\ \Lambda_N(r_E,\vartheta,R_{E,N},\omega_N)\end{bmatrix} &= \begin{bmatrix}B_{E,0}^1 & B_{E,1}^1 & B_{E,2}^1 & B_{E,3}^1\cdots\\ B_{E,0}^2 & B_{E,1}^2 & B_{E,2}^2 & B_{E,3}^2\cdots\\ \vdots & \vdots & \vdots & \vdots\\ B_{E,0}^N & B_{E,1}^N & B_{E,2}^N & B_{E,3}^N\cdots\end{bmatrix}\begin{bmatrix}F_{E,0}\\ F_{E,1}\\ F_{E,2}\\ F_{E,3}\\ \vdots\end{bmatrix}\\ &= \mathbf{B}_{E,\infty}(\mathbf{R}_E,\boldsymbol{\omega})\mathbf{F}_{E,\infty}(r_E,\vartheta),\end{aligned} \qquad (21)$$

where

$$B_{E,i}^j = \left[Ce_i^e \mathrm{Se}_i^e(q,\omega_j) \quad Ce_i^o \mathrm{Se}_i^o(q,\omega_j) \quad Co_i^e \mathrm{So}_i^e(q,\omega_j) \quad Co_i^o \mathrm{So}_i^o(q,\omega_j)\right],$$

$$F_{E,i} = \begin{bmatrix} {\mathrm{Re}^{(1)}}_i^e(q,r_E)\mathrm{Se}_i^e(q,\vartheta)/Le_i^{e*} \\ {\mathrm{Re}^{(1)}}_i^o(q,r_E)\mathrm{Se}_i^o(q,\vartheta)/Le_i^{o*} \\ {\mathrm{Ro}^{(1)}}_i^e(q,r_E)\mathrm{So}_i^e(q,\vartheta)/Lo_i^{e*} \\ {\mathrm{Ro}^{(1)}}_i^o(q,r_E)\mathrm{So}_i^0(q,\vartheta)/Lo_i^{o*} \end{bmatrix}, \; Ls_n^{t*} = \max_{r\in[r_D,R_D]} |{\mathrm{Rs}^{(1)}}_n^t(q,r)|, \; s,t = [e,o], \tag{22}$$

$r_D$and R_D are defined in (8), and

$$\begin{cases} Ce_n^e = \dfrac{4{\mathrm{Re}^{(3)}}_n^e(q,R_E)}{Ne_n^e} Le_n^{e*}, \\[2ex] Ce_n^o = \dfrac{4{\mathrm{Re}^{(3)}}_n^o(q,R_E)}{Ne_n^o} Le_n^{o*}, \\[2ex] Co_n^e = \dfrac{4{\mathrm{Ro}^{(3)}}_n^e(q,R_E)}{No_n^e} Lo_n^{e*}, \\[2ex] Co_n^o = \dfrac{4{\mathrm{Ro}^{(3)}}_n^o(q,R_E)}{No_n^o} Lo_n^{o*}, \end{cases}$$

for $n, i = 0, 1, ...$ and $j = 1, 2, ..., N$.

Truncating the series expansion (20) for some $T_E \in \mathbb{N}$ satisfying $4T_E \geq N$, we get

$$\Xi(r_E, \vartheta, \mathbf{R}_E, \boldsymbol{\omega}) = \mathbf{B}_E(\mathbf{R}_E, \boldsymbol{\omega})\mathbf{F}_E(r_E, \vartheta), \tag{23}$$

which is analogous to (9). From (23) we proceed as in section 3 to obtain the new basis functions.

The computational implementation of the MFS-SVD remains similar to the classic MFS, with an additional SVD decomposition and a matrix multiplication as in (12). Also, one needs to take into account the truncation of the series in (6), that defines the precision of the approximation of the fundamental solution and the dimensions of the matrices $\mathbf{B}$ and $\mathbf{F}$ in (7) and (21), that though do not have a higher implementation complexity, increase the computation cost of the MFS-SVD in comparison with the classic MFS. The algorithm that summarizes the implementation of this technique is described in [1]. In our case we need to remove steps 5, 6 and 7 of that algorithm and consider the notations introduced here. Regarding the computation time, we have observed much higher computational cost of the MFS-SVD compared to the classic MFS. The increase in the computation cost comes from the SVD decomposition, which is aggravated in the MFS-SVD$_E$ due to the larger matrices, as well as the evaluation of the Mathieu functions. A comparison of the CPU time in some cases, is provided in next section (see Tables 1 and 2) with the computations being carried on a desktop computer with processor Intel(R) Core(TM) i5-4460T CPU @1.9GHz and 4.00 Gb of RAM.

5. Numerical Results

Let us illustrate the feasibility of the proposed method by considering different cases with circular, elliptic and other domains. To evaluate the performance of the proposed methods, in some examples we compute the L^2-norm $||u - u_N^{SVD}||_{L^2(D)}$ in the interior of D and in others the L^2-norm $||g - u_N^{SVD}||_{L^2(\partial D)}$ on its boundary.

In all cases, the source points are distributed in an equiangular way.

5.1. MFS-SVD in polar coordinates

The approximations for the J_n^* defined in (8) were obtained as in [16] by simply evaluating $|J_n^*|$ at 10000 equally spaced points $r_i \in [r_D, R_D]$ and taking their maximum. In the context of Remark 1, to overcome underflow problems while computing the ratio J_n/J_n^*, we use a threshold of $N^* = 140$ since it is the first n that returns $J_n(1) = 0$.

5.1.1. Disk

Following an example considered in [16], we consider a problem in the unit disk with exact solution

$$u(x) = -\frac{1}{4} Y_0(k|x - (x_0, 0)|), \quad x \in \bar{D}, \quad x_0 > 1.$$

We take the wavenumber $k = 8$ and we place the source points in a circumference with radius $R = 1.5$ centered at origin. We look for approximations in the cases $x_0 = 3$ and $x_0 = 1.1$, outside and inside the circle defined by the source points. Figure 1 shows the results for the case $x_0 = 3$ with both approaches, namely the MFS-DIR and the proposed MFS-SVD$_P$. In this case both approaches have similar behavior, whatever the number of source points considered, and in both cases around $N = 70$ source points are sufficient to reach machine precision. However, the similarities in the results are not observed in the computation time where the MFS-SVD$_P$ is by far more expensive than the MFS-DIR, Table 1. The second case $x_0 = 1.1$ is more challenging, since the solution cannot be analytically extended to the artificial boundary C. We consider approximations for $R = 1.05$ and $R = 1.5$, since it is known that the MFS-DIR performs better when the artificial boundary is close to the domain. Figure 2 illustrates this behavior with an error of order 10^{-13} for $R = 1.05$ against 10^{-6} for $R = 1.5$ when we consider 400 collocation points. On the other hand the MFS-SVD$_P$ has similar behavior in both cases which is similar to the best MFS-DIR case. Figure 2 also justifies the previous results by illustrating the evolution of the condition number (middle) and the effective condition number (right) in the considered cases. While for MFS-SVD$_P$ it remains bounded, it explodes for the MFS-DIR, namely in the case for $R = 1.5$. .

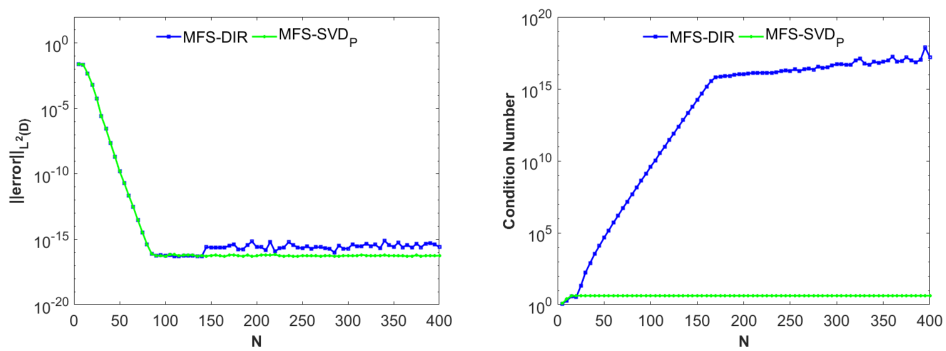

Figure 1: MFS-SVD$_P$ vs. MFS-DIR for the Helmholtz equation with unit disk as domain, exact solution $u(x) = -\dfrac{1}{4}Y_0(k|x-\gamma|)$, with $\gamma = (3,0)$, $k = 8$ and source points in a circumference with $R = 1.5$. Plot of the error in the domain (left) and condition number (right).

Table 1: Computation time, in seconds, as a function of collocation points for the case considered in Figure 1.

N	**MFS-DIR**	**MFS-SVD$_P$**
5	0.097	450.494
100	0.893	717.109
200	2.063	1001.109

The previous example illustrates that MFS-SVD$_P$ behaves better than the MFS-DIR for large N. To further test the robustness of this approach we consider another example from [16]. Again the exact solution is known and given by $u(r,\theta) =$

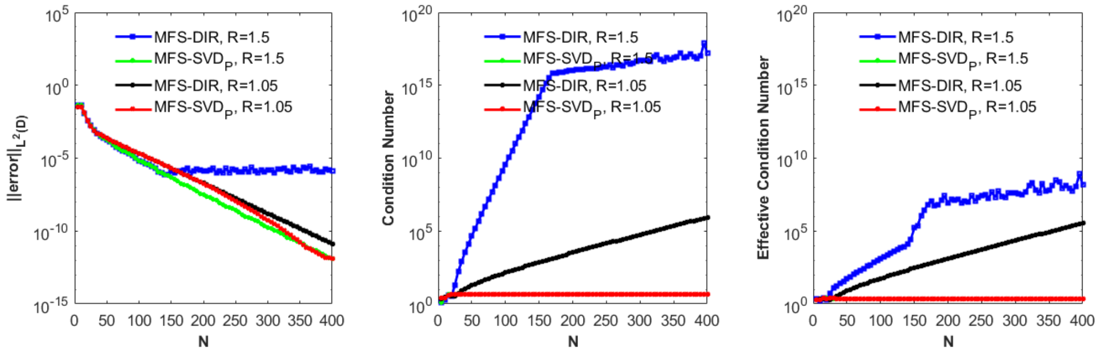

Figure 2: MFS-SVD$_P$ vs. MFS-DIR for the Helmholtz equation with unit disk as domain, exact solution $u(x) = -\frac{1}{4}Y_0(k|x-\gamma|)$, with $\gamma = (1.1, 0)$, $k = 8$ and source points in a circumference with $R = 1.05$ and $R = 1.5$. Plot of the error in the domain (left), condition number (center) and effective condition number (right).

$e^{im\theta} J_m(kr)/J_m(k), m \in \mathbb{N}$. We first fix $m = 2$ and look for approximations to cases with wavenumber $k = 1, 10, 100$, (see Figure 3). We can observe a similar behavior of the error for both approaches with minor improvements for the MFS-SVD$_P$, with a much better conditioning. In the second scenario we fix $k = 1$ and we explore the approximations for $m = 10, 30, 50$ with results presented in Figure 4. For this scenario we see clearly the MFS-SVD$_P$ performing better than the classic approach; we have the approximations reaching machine precision in all cases, at the cost of increasing source points as m increases, but the MFS-DIR shows results deteriorating from machine precision order in $m = 10$ to an error around 10^{-4} in the case $m = 50$. In both scenarios we can observe the boundedness of the condition number of the MFS-SVD$_P$.

Remark 2. The MFS-SVD$_P$ is based on expansion (7) which is afterwards truncated for $T_P \in \mathbb{N}$, with $2T_P + 1 \geq N$. The selection of T_P should be made carefully. In fact, increasing the value of T_P does not always translate in better approximations, due to the numerical computations of the truncated version of (6). In each case, the choice of source points and the guarantee of machine precision in (7) should define the value of T_P.

5.1.2. Ellipse

Next we analyze the performance of the method in case of elliptic domains. Let us consider the elliptic boundary domain given by the equation $x^2/a^2 + y^2 = 1$. This case was considered in [30] for $a = 2$ and in [16] for $a = 2, 3, .., 7$, with the boundary

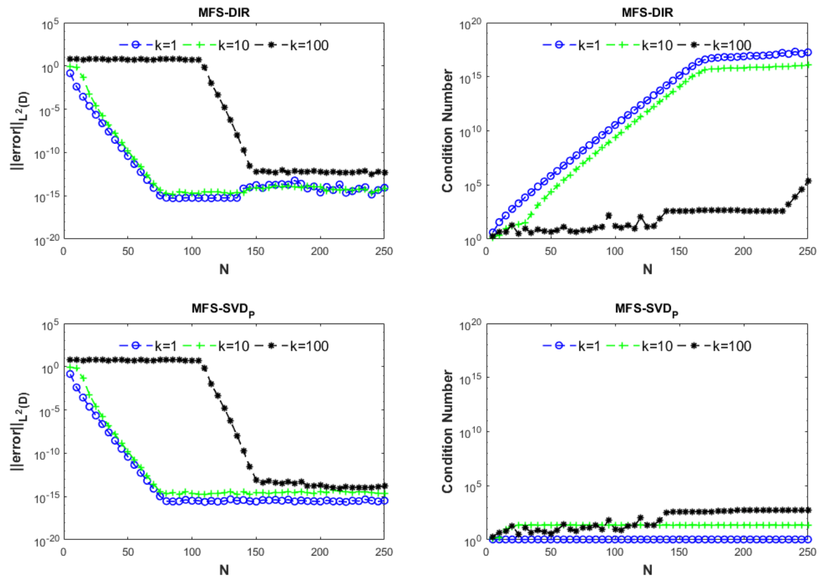

Figure 3: Plot of the error in the domain and condition number of the MFS-DIR (first line) and MFS-SVD$_P$ (second line) for the Helmholtz equation with unit disk as domain, exact solution $u(r,\theta) = e^{im\theta}J_m(kr)/J_m(k)$, $k = 1, 10, 100$, $m = 2$ and the circumference with $R = 1.5$ as artificial boundary.

values given by $g(x,y) = e^{i(x^2+y^2)}\sin(x+y)$. Let us take $k = 1$ and $a = 6$; first we place the source points on a circumference of radius $R = 50$ centered at the origin, a situation where the classical MFS shows poor performance, with results in Figure 5; secondly, we consider the source points to be on an ellipse with semiaxes multiplied by 10, results in Figure 8. We can see that, no matter where the source points are located the classical approach always shows an error of order 1; in contrast the MFS-SVD$_P$ approach shows slightly better results with error of order 10^{-4}, as the evolution of the condition number is slightly different when compared to the classical approach. However, in both cases we do not manage to control the condition number as in the disk case nor achieve machine precision accuracy.

5.1.3. Square

To finalize this section let us consider a non smooth domain, the square with side length equal to 1. The source points and the collocation points are distributed as in previous cases. The wavenumber and the values at the boundary are taken as in Example 5.1.2. As artificial boundary we consider two cases, a circumference with

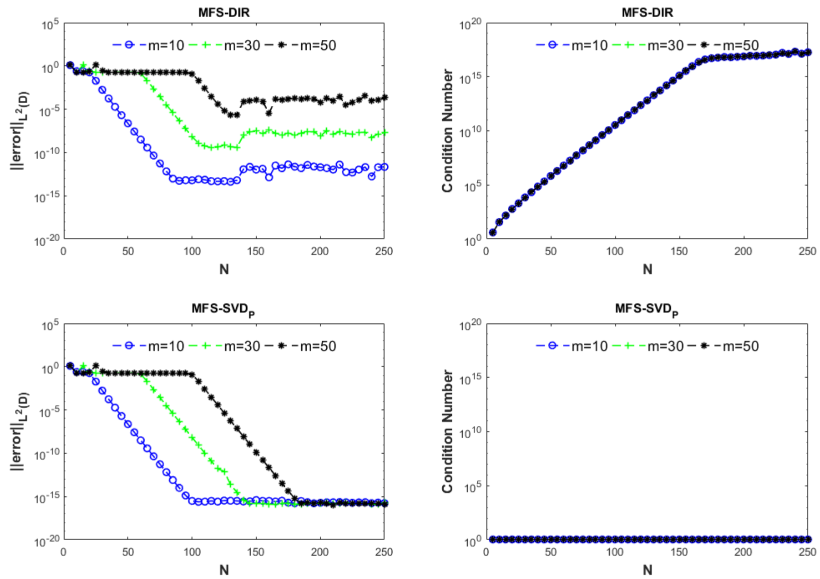

Figure 4: Plot of the error in the domain and condition number of the MFS-DIR (first line) and MFS-SVD$_P$ (second line) for the Helmholtz equation with unit disk as domain, exact solution $u(r, \theta) = e^{im\theta} J_m(kr)/J_m(k)$, $m = 10, 30, 50$, $k = 1$ and the circumference with $R = 1.5$ as artificial boundary.

radius $R = 5$ and the square with side length equal to 3. The results are presented in Figure 6 and no matter the artificial boundary considered still the MFS-SVD$_P$ performs better than the MFS-DIR; the improvement is not that pronounced as in the disk case but still the MFS-SVD$_P$ has the condition number increasing in a slower pace than in the MFS-DIR which results in improvements in accuracy. An important remark is that we have observed that to obtain good results with MFS-SVD$_P$ the set of collocation points should always include the corners of the square.

5.2. MFS-SVD in elliptic coordinates

The previous results on the elliptic domain show that the MFS-SVD$_P$, does not address properly the problem of improving the conditioning, even though the results are better than for the MFS-DIR. Let us now illustrate the performance of the proposed method when using the elliptic coordinates formulation of the MFS-SVD described in section 4.

In the elliptic coordinates case the approximations for Ls_n^{t*}, defined in (22), were obtained, as in the polar case, by simply evaluating $|\mathrm{Rs}^{(1)}{}_n^t(q, r)|$ at 10000 equally

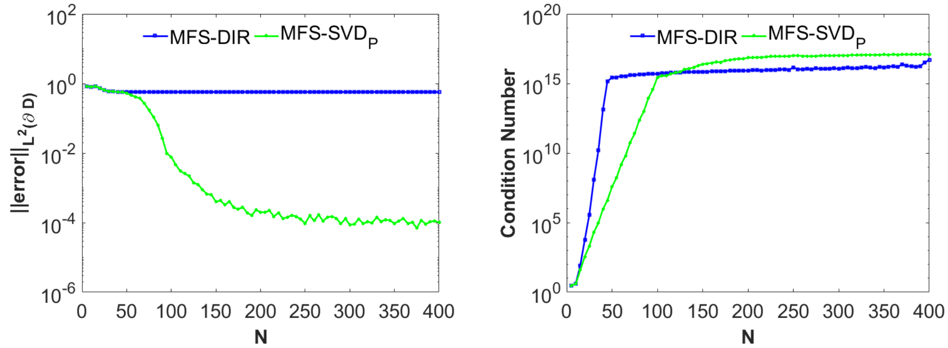

Figure 5: MFS-SVD$_P$ vs. MFS-DIR for the Helmholtz equation on an elliptic domain given by $x^2/6^2 + y^2 = 1$ with source points on a circumference with $R = 50$, boundary values given by $g(x, y) = e^{i(x^2+y^2)} \sin(x+y)$. Plot of the error on the boundary (left) and condition number (right).

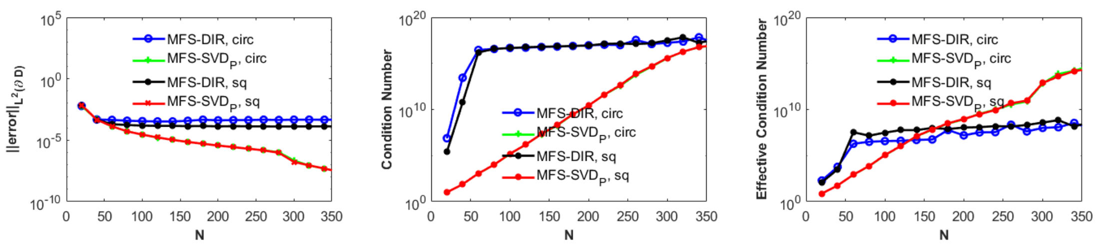

Figure 6: MFS-SVD$_P$ vs. MFS-DIR for the Helmholtz equation on a square domain with side length equal to 1, source points on a circumference with $R = 5$ and on a square with side length equal to 3, with boundary values given by $g(x, y) = e^{i(x^2+y^2)} \sin(x + y)$. Plot of the error on the boundary (left), condition number (center) and effective condition number (right).

spaced points $r_i \in [r_D, R_D]$ and taking their maximum. In the following example, as we consider the case of two confocal ellipses, one representing the domain under study and the other the closed curve containing the source points, we simply evaluate $|\mathrm{Rs}^{(1)}{}^t_n(q, r)|$ at $r = r_E$ since in the elliptic coordinate system $r_D = R_D$.

Remark 3. The numerical implementation is being carried out using Matlab which does not have Mathieu functions implemented; to evaluate these functions we used the toolbox "Matlab Mathieu Functions Toolbox v.1.0 ", [31, 32], with a few modifications to increase the accuracy. The main modification performed in that code is on the definition of the radial Mathieu functions. These functions have in their definitions an offset integer parameter s for the order of the Bessel functions. This parameter is set by default equal to 0 for the even-even, even-odd and odd-odd, radial functions and set to 1 for the odd-even in the above toolbox. This somehow traditional selection of values for the parameter s is known to provide acceptable results, namely single precision accuracy, when n is not large [33]; for high values of n one can find the evaluation errors increasing without bound. Since for the proposed MFS-SVD approach the number of collocation points depends on the number of terms used to truncate the series (20) single precision accuracy is not satisfactory, and we have therefore modified the code in order to allow a better parameter choice and therefore improve the accuracy to double precision.

It has been observed that the use of larger offset values tends to improve the accuracy [34]. We have therefore performed a modification of Cojocaru's code by introducing the possibility to change the offset parameter s and we select this parameter by considering the ideas of the "tuning algorithm" described in [33]. In Figure 7 we illustrate the improvement we can get after this modification by considering the following example; in (20) we take $x = (6, 0)$, $y = (16.45904993363967, 0)$ and $q = 8.75$. The elliptic coordinates for x, y are $(0.1682361183106064, 0)$ and $(1.682361183106065, 0)$, respectively. We evaluate the L^2-error between the fundamental solution computed by Matlab built-in functions and the evaluation using (20). As we can see by using the original toolbox we would be limited to truncating the series around $n = 10$ as we get the best accuracy at this point. However, truncating at this level would give us only a maximum of $N = 40$ source points which can be very low to achieve good approximations. After the modification of the code we can reach machine precision accuracy and stability with increasing N.

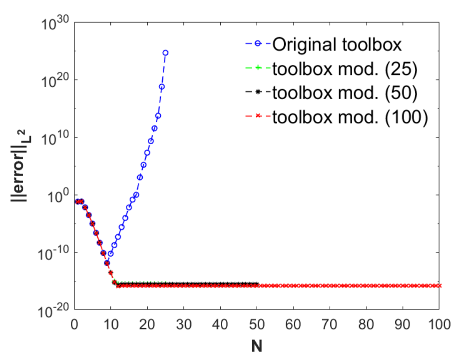

Figure 7: L^2-error before and after modification of Cojocaru's toolbox, for the particular case given by cartesian coordinates $x = (6, 0)$, $y = (16.45904993363967, 0)$, the corresponding elliptic coordinates are $(0.1682361183106064, 0)$,$(1.682361183106065, 0)$, with $q = 8.75$. The original code only consider a maximum of 25 terms in Mathieu functions. The modified code was tested with 25, 50 and 100 terms.

5.2.1. Ellipse

We take the same example considered in subsubsection 5.1.2. First we illustrate, by considering as artificial boundary an ellipse magnified by different factors 1.05, 2.1, 3.15, 4.20, 5.25 and 10. From Figure 8 (left) we observe that in this particular case the location of the artificial boundary does not seem to improve that much the accuracy of the MFS-DIR. On the other side Figure 8 (center and right) shows the comparison between both MFS-SVD approaches versus the MFS-DIR considered only for artificial boundary magnified by 10. Clearly we can see that the elliptic coordinates formulation is better when considering elliptic domains. We have the error of MFS-SVD$_E$ reaching order 10^{-14} while the MFS-SVD$_P$ stabilizes at order 10^{-4} and the MFS-DIR at order 1. Again the computational performance is the main drawback of the this approach as we can observe in Table 2.

Table 2: Computation time, in seconds, as a function of the collocation points, for the case considered in Figure 8.

N	**MFS-DIR**	**MFS-SVD$_P$**	**MFS-SVD$_E$**
5	0.065	387.648	3958.186
100	0.331	505.707	5052.500
200	0.712	634.791	39 118.740

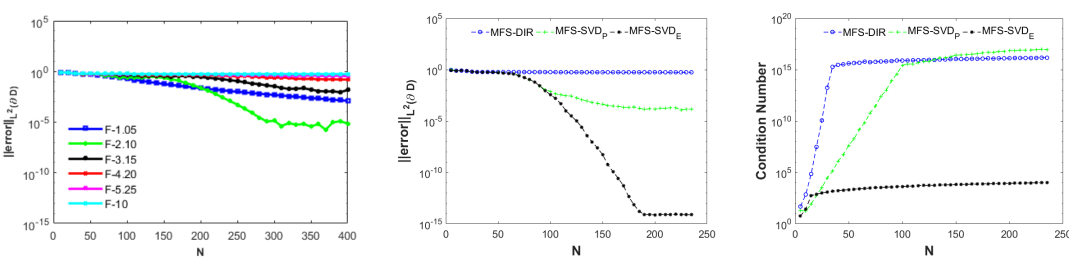

Figure 8: MFS-DIR for different artificial boundary obtained by using different magnified factors (left). Comparison between MFS-DIR, MFS-SVD$_P$ and MFS-SVD$_E$, for the Helmholtz equation on an elliptic domain given by $x^2/6^2+y^2=1$ with source points on an ellipse with semiaxes multiplied by 10, boundary values given by $g(x,y)=e^{i(x^2+y^2)}\sin(x+y)$. Plot of the error on the boundary (center) and condition number (right).

5.2.2. Peanut-shaped smooth domain

We now consider the peanut-shaped domain in [35] a non elliptic domain elongated in the x-axis direction, with boundary ∂D illustrated in Figure 9 (left), described by the parametrization

$$\partial D = \left\{ 3\sqrt{\cos^2(t) + 0.25\sin^2(t)}\{\cos(t), \sin(t)\}, \quad t \in [0, 2\pi[\right\}.$$

To evaluate the performance of the MFS-SVD$_E$ we consider three cases: (a) The case with boundary values given by $g(x,y) = e^{i(x^2+y^2)}\sin(x+y)$, (b) the case with exact solution $u(x,y) = -\dfrac{1}{4}Y_0(k|(x,y)-\gamma|)$ with $\gamma = (5,0)$ and $\gamma = (400,0)$ at inside and outside the domain defined by the artificial boundary, respectively and (c) the plane wave $u(x,y) = e^{ik(x+y)/\sqrt{2}}$.

In all cases the artificial boundary is an ellipse, the points will be distributed as in the previous cases and we consider the wavenumber $k = 1$. Note that in the case with two confocal ellipses the elliptic coordinate system was defined using the parameter σ in (18), given by the ellipse which defines the domain; in this case σ is defined from the ellipse with semiaxes a and b given by the distance between the origin and the intersection of the peanut-shaped curve with the x-axes and y-axes respectively, i.e. $a = 3$ and $b = 1.5$.

The numerical results for case (a) are presented in Figure 9, for case (b) in Figures 10-11 and for case (c) in Figure 12. In all cases we clearly see an improvement of the conditioning when using the MFS-SVD$_P$ approach and even more when considering the MFS-SVD$_E$, as expected. We can observe as well that even though the MFS-SVD$_P$ shows better conditioning at the beginning when compared to the MFS-DIR, the condition number still grows relatively fast to reach an order of 10^{15} or higher in all cases; as illustrated in Figure 9 this is limiting the improvement of the accuracy of the MFS-SVD$_P$ and even deteriorating it as the condition number surpasses 10^{15}. On the other hand the MFS-SVD$_E$ shows a slowly growing condition number, which allows for an improvement in accuracy.

6. Conclusions

In this work two extensions of [1] are presented. First extension is to check whether this approach would perform as well as in the Laplace case for other physical problems. Indeed we have illustrated that the MFS-SVD$_P$ applied to the Helmholtz equation in $\mathbb{R}^2$ performs as well as observed in the Laplace equation . Second we recall that it has already been observed that for non circular domains we do have improvements on accuracy but the condition number is not as well controlled as in domains close to a disk, therefore limiting the improvements on the accuracy in certain cases. For this reason we have addressed the question of improving the conditioning of the matrix, for elliptic boundaries, by proposing the MFS-SVD$_E$. This

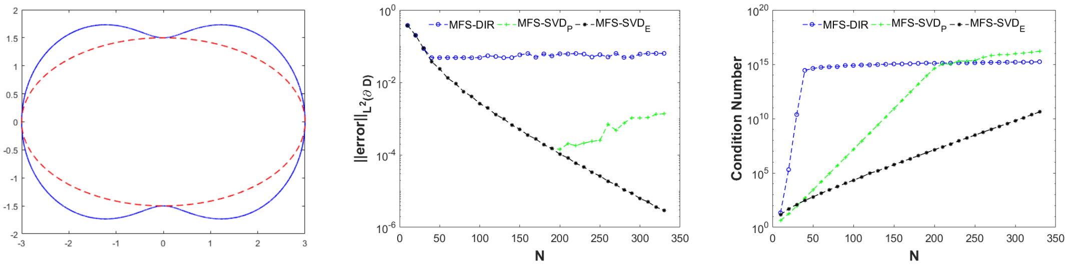

Figure 9: Peanut-shaped domain and the ellipse which defines the elliptic coordinates system (left). Comparison between MFS-DIR, MFS-SVD$_P$ and MFS-SVD$_E$, for the Helmholtz equation on a peanut domain with source points on an ellipse, semiaxes multiplied by 10, boundary values given by $g(x, y) = e^{i(x^2+y^2)} \sin(x + y)$. Plot of the error on the boundary (center) and condition number (right).

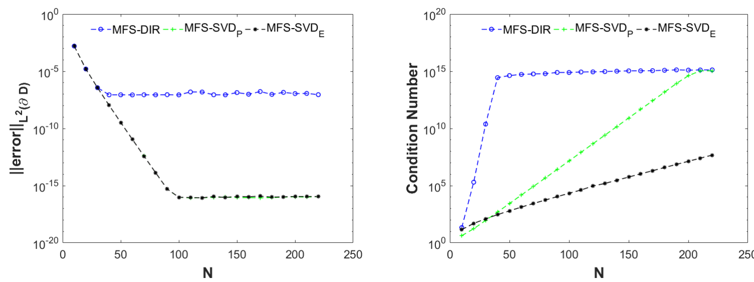

Figure 10: Comparison between MFS-DIR, MFS-SVD$_P$ and MFS-SVD$_E$, for the Helmholtz equation on peanut a domain with source points on an ellipse, semi-axes multiplied by 10, exact solution $u(x) = -\frac{1}{4}Y_0(k|x-\gamma|)$, $\gamma = (5, 0)$ and $k = 1$. Plot of the error on the boundary (left) and condition number (right).

was achieved by introducing the Mathieu functions as basis functions to represent the solutions in this domain instead of Bessel functions which better fit the problems with disks. Our work shows that by following this approach we can effectively control the condition number and therefore improve the accuracy, being able to use a higher number of source and collocation points without compromising the conditioning of the linear system.

Another contribution of this work is on the discussion about the numerical evaluation of Mathieu functions. These functions sometimes considered by some authors as intractable, and many times reported as showing important cancellation errors, are recognized as the ideal functions to address problems involving elliptic domains. We have illustrated, that we can use Mathieu functions and get very good results, all this due to the adaptation of a previous code, allowing for a better choice

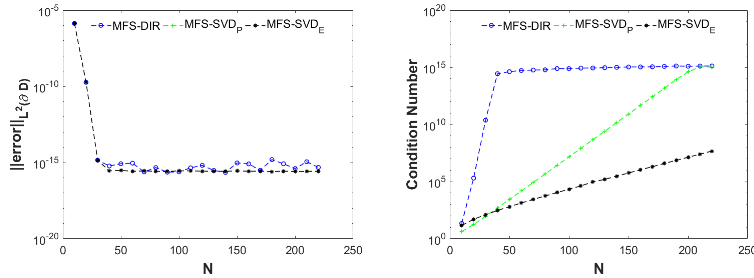

Figure 11: Comparison between MFS-DIR, MFS-SVD$_P$ and MFS-SVD$_E$, for the Helmholtz equation on a peanut domain with source points on an ellipse, semi-axes multiplied by 10, exact solution $u(x) = -\frac{1}{4}Y_0(k|x-\gamma|)$, $\gamma = (400, 0)$ and $k = 1$. Plot of the error on the boundary (left) and condition number (right).

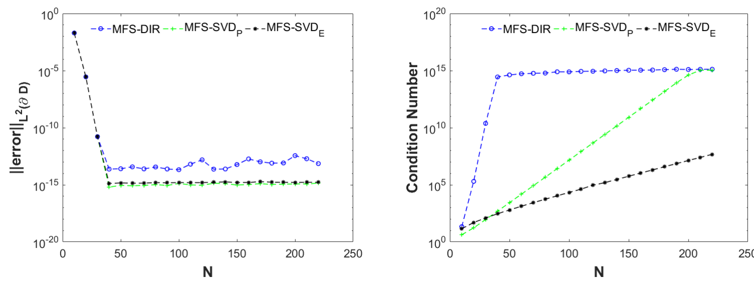

Figure 12: Comparison between MFS-DIR, MFS-SVD$_P$ and MFS-SVD$_E$, for the Helmholtz equation on peanut domain with source points on an ellipse, semi-axes multiplied by 10, boundary values given by $u(x,y) = e^{ik(x+y)/\sqrt{2}}$ and $k = 1$. Plot of the error on the boundary (left) and condition number (right).

of the parameter s for each case.

The proposed extension of [1] reinforces the idea that the MFS-SVD is suited for several boundary value problems. Therefore our future work will focus on illustrating this case, namely by assessing the MFS-SVD performance for the Helmholtz equation in $\mathbb{R}^3$ the propagation of elastic waves in $\mathbb{R}^2$ and $\mathbb{R}^3$, for instance.

Acknowledgments

The research of Pedro R. S. Antunes and Hernani Calunga is partially supported by FCT, Portugal, through the scientific project UIDB/00208/2020.

The research of Pedro Serranho is partially funded by FCT throught the projects UIDB/04950/2020, UIDP/04950/2020, UIDB/04621/2020 and UIDP/04621/2020.

7. Appendix

7.1. Definition of angular, radial and normalization factor for Mathieu functions following Stratton convention

Knowing that A_{**} are the Mathieu expansion coefficients then the angular Mathieu funcions can be represented in terms of sine and cosine and the radial Mathieu functions in terms of products of Bessel functions defined by, [29, 33]

$$Ne^e_n = 2\pi\Bigg(\sum_{j=0}^{\infty} A^{(0)}_{ee}(q,n)\Bigg)^2 + \pi\Bigg(\sum_{j=1}^{\infty} A^{(2j)}_{ee}(q,n)\Bigg)^2,\ Ne^o_n = \pi\Bigg(\sum_{j=0}^{\infty} A^{(2j+1)}_{eo}(q,n)\Bigg)^2,$$

$$No^o_n = \pi\Bigg(\sum_{j=0}^{\infty} A^{(2j+1)}_{oo}(q,n)\Bigg)^2, \quad No^e_n = \pi\Bigg(\sum_{j=1}^{\infty} A^{(2j)}_{oe}(q,n)\Bigg)^2,$$

$$\mathrm{Se}^e_n(u,q) = \sum_{j=0}^{\infty} A^{(2j)}_{ee}(q,n)\cos(2ju), \quad \mathrm{Se}^o_n(u,q) = \sum_{j=0}^{\infty} A^{(2j+1)}_{eo}(q,n)\cos((2j+1)u),$$

$$\mathrm{So}^o_n(u,q) = \sum_{j=1}^{\infty} A^{(2j)}_{oe}(q,n)\sin(2ju), \quad \mathrm{So}^o_n(u,q) = \sum_{j=0}^{\infty} A^{(2j+1)}_{oo}(q,n)\sin((2j+1)u),$$

$$\mathrm{Re}^{(1,2)}{}^e_n(u,q) = \sqrt{\frac{\pi}{2}}\frac{(-1)^r}{A^{(2s)}_{(ee)}(q,n)} Mc^{(1,2)}_{ee}(u,q), \quad r = t/2 \quad t = 0, 2, 4, ...,$$

$$\mathrm{Re}^{(1,2)}{}^o_n(u,q) = \sqrt{\frac{\pi}{2}}\frac{(-1)^r}{A^{(2s+1)}_{(eo)}(q,n)} Mc^{(1,2)}_{eo}(u,q), \quad r = (t-1)/2 \quad t = 1, 3, 5, ...,$$

$$\mathrm{Ro}^{(1,2)}{}^e_n(u,q) = \sqrt{\frac{\pi}{2}}\frac{(-1)^r}{A^{(2s)}_{(oe)}(q,n)} Ms^{(1,2)}_{oe}(u,q), \quad r = t/2 \quad t = 2, 4, 6, ...,$$

$$\mathrm{Ro}^{(1,2)}{}^o_n(u,q) = \sqrt{\frac{\pi}{2}}\frac{(-1)^r}{A^{(2s+1)}_{(oo)}(q,n)} Ms^{(1,2)}_{oo}(u,q) \quad r = (t-1)/2 \quad t = 1, 3, 5, ...,$$

$$\mathrm{Re}^{(3)}_n(u,q) = \mathrm{Re}^{(1)}_n(u,q) + i\mathrm{Re}^{(2)}_n(u,q), \quad \mathrm{Ro}^{(3)}_n(u,q) = \mathrm{Re}^{(1)}_n(u,q) + i\mathrm{Ro}^{(2)}_n(u,q)$$

with,

$$
\begin{aligned}
Mc_{ee}^{(p)} &= \sum_{j=0}^{\infty}(-1)^j A_{ee}^{(2j)}(q,n)\Big(J_{k-s}(v_1)Z_{k+s}^{p}(v_2) + J_{k+s}(v_1)Z_{k-s}^{p}(v_2)\Big),\\
Mc_{eo}^{(p)} &= \sum_{j=0}^{\infty}(-1)^j A_{eo}^{(2j+1)}(q,n)\Big(J_{k-s}(v_1)Z_{k+s+1}^{p}(v_2) + J_{k+s+1}(v_1)Z_{k-s}^{p}(v_2)\Big),\\
Ms_{oe}^{(p)} &= \sum_{j=1}^{\infty}(-1)^j A_{oe}^{(2j)}(q,n)\Big(J_{k-s}(v_1)Z_{k+s}^{p}(v_2) - J_{k+s}(v_1)Z_{k-s}^{p}(v_2)\Big),\\
Ms_{oo}^{(p)} &= \sum_{j=0}^{\infty}(-1)^j A_{oo}^{(2j+1)}(q,n)\Big(J_{k-s}(v_1)Z_{k+s+1}^{p}(v_2) - J_{k+s+1}(v_1)Z_{k-s}^{p}(v_2)\Big)
\end{aligned}
$$

where, $v_1 = \sqrt{q}\,e^{-u}$, $v_2 = \sqrt{q}\,e^{u}$, $Z^1 = J$, $Z^2 = Y$ and s is an arbitrary integer parameter.

References

[1] P. R. S. Antunes, A well-conditioned method of fundamental solutions for Laplace equation, Numerical Algorithms 91 (2022) 1381–1405.

[2] V. D. Kupradze, M. A. Aleksidze, The method of fundamental equations for the approximate solution of certain boundary value problems, U.S.S.R. Computational Mathematics and Mathematical Physics 4 (1964) 82–126.

[3] A. H. Barnett, T. Betcke, Stability and convergence of the method of fundamental solutions for Helmholtz problems on analytic domains, Journal of Computational Physics 227(14) (2008) 7003–7026.

[4] C. J. S. Alves, A. L. Silvestre, Density results using Stokeslets and a method of fundamental solutions for the Stokes equations, Engineering Analysis with Boundary Elements 28 (2004) 1245–1252.

[5] A. Karageorghis, D. Lesnic, The method of fundamental solutions for the Oseen steady-state viscous flow past known or unknown shapes, Numerical Methods for Partial Differential Equations 35 (2009) 2103–19.

[6] J. R. Berger, A. Karageorghis, The method of fundamental solutions for layered elastic materials, Engineering Analysis with Boundary Elements 25 (2001) 877–86.

[7] Q. G. Liu, B. Sarles, A non-singular method of fundamental solutions for the two-dimensional steady-state isotropic thermoelasticity problems, Engineering Analysis with Boundary Elements 75 (2017) 89–102.

[8] C. J. S. Alves, P. R. S. Antunes, The method of fundamental solutions applied to some inverse eigenproblems, SIAM Journal on Scientific Computing 35 (2013) A1689–A1708.

[9] C. S. Chen, S. Y. Reutskiy, V. Y. Rozov, The method of fundamental solutions and its modifications for electromagnetic field problems, Computer Assisted Methods in Engineering and Science 16 (2009) 21–33.

[10] D. L. Young, J. W. Ruan, Method of fundamental solutions for scattering problems of electromagnetic waves, Computer Modelling in Engineering & Sciences 7(2) (2005) 223–32.

[11] J. R. Berger, A. Karageorghis, The method of fundamental solutions for heat conduction in layered materials, Numerical Methods in Engineering 45 (1999) 1681–1694.

[12] C. C. Tsai, D. L. Young, J. H. Chiang, D. C. Lo, The method of fundamental solutions for solving options pricing models, Applied Mathematics and Computation 45 (2006) 390–401.

[13] L.-P. Zhang, Z.-C. Li, Y. Wei, H.-T. Huang, New regularization techniques for ill-conditioning problems and their applications: Choices of regularization parameters, Engineering Analysis with Boundary Elements 61 (2015) 91–103.

[14] P. A. Ramachandran, Method of fundamental solutions: singular value decomposition analysis, Numerical Methods in Biomedical Engineering 18 (2002) 789–801.

[15] G. Feng, M. Li, C. S. Chen, On the ill-conditioning of the MFS for irregular boundary data with sufficient regularity, Engineering Analysis with boundary elements 18 (2014) 98–102.

[16] P. R. S. Antunes, A numerical algorithm to reduce ill-conditioning in meshless methods for the Helmholtz equation, Numerical Algorithms 79(3) (2018) 879–897.

[17] P. R. S. Antunes, Reducing the ill conditioning in the method of fundamental solutions, Advances in Computational Mathematics 44 (2018) 351–365.

[18] L.-P. Zhang, Z.-C. Li, Y. Wei, H.-T. Huang, New regularization techniques for ill-conditioning problems and their applications: Choices of regularization parameters, Engineering Analysis with Boundary Elements 152 (2023) 347–361.

[19] A. Bogomolny, Fundamental solutions method for elliptic boundary value problems, SIAM Journal on Numerical Analysis 22(4) (1985) 644–669.

[20] G. Fairweather, A. Karageorghis, The method of fundamental solutions for elliptic boundary value problems, Advances in Computational Mathematics 9(1) (1998) 69–95.

[21] R. Mathon, R. L. Johnston, The approximate solution of elliptic boundary-value problems by fundamental solutions, SIAM Journal on Numerical Analysis 14(4) (1977) 638–650.

[22] Y.-S. Smyrlis, Applicability and applications of the method of fundamental solutions, Mathematics of Computation 78 (2009) 1399–1434.

[23] Y.-S. Smyrlis, A. Karageorghis, Efficient implementation of the MFS: the three scenarios, Journal of Computational and Applied Mathematics 227(1) (2009) 83–92.

[24] D. Colton, R. Kress, Inverse acoustic and electromagnetic scattering theory, Applied Mathematics Sciences 93 (2010).

[25] M. Abramowitz, I. A. Stegun, Handbook of mathematical functions with formulas, graphs and mathematical tables, Applied Mathematics series 55 (1964) 365.

[26] Z.-C. Li, L.-P. Zhang, Y. Wei, M.-G. Lee, J. Y. Chiang, Boundary methods for dirichlet problems of Laplace's equation in elliptic domains with elliptic holes, Engineering Analysis with Boundary Elements 61 (2015) 91–103.

[27] L. Zhang, Z.-C. Li, H.-T. Huang, M.-G. Lee, Comparisons of method of fundamental solutions, method of particular solutions and the MFS-QR; stability analysis, Engineering Analysis with Boundary Elements 123 (2021) 182–199.

[28] P. M. Morse, H. Feshbach, Methods of theoretical physics, McGraw-Hill Company, Inc. (1953).

[29] D. Erricolo, Acceleration of the convergence of series containing Mathieu functions using shanks transformation, IEEE Antennas and Wireless Propagation Letters 2 (2003) 58–61.

[30] C. J. S. Alves, S. S. Valtchev, Numerical comparison of two meshfree methods for acoustic waves scattering, Engineering Analysis with Boundary Elements 29(4) (2005) 371–382.

[31] E. Cojocaru, Mathieu functions toolbox v.1.0, `https://www.mathworks.com/matlabcentral/fileexchange/22081-mathieu-functions-toolbox-v-1-0,MATLABCentralFileExchange.RetrievedOctober9,2023` (2008).

[32] E. Cojocaru, Mathieu functions computational toolbox implemented in Matlab, `arXiv:0811.1970v2` (2008).

[33] M. M. Bibby, A. F. Peterson, Accurate computation of Mathieu functions, Synthesis Lectures on Computational Electromagnetics (2013).

[34] A. L. V. Buren, J. E. Boisvert, Accurate calculation of modified Mathieu functions of integer order, Quarterly of Applied Mathematics 65 (2007) 1–23.

[35] P. Serranho, A hybrid method for inverse scattering for shape and impedance, Inverse Problems 22 (2006) 663–680.